# Short Papers

## Modal Analysis of the "Gap Effect" in Waveguide Dielectric Measurements

SCOTT B. WILSON

*Abstract* — **In waveguide measurements on dielectric slabs, small air gaps between the guide walls and the dielectric sample are found to be capable of radically altering the complex reflection and transmission coefficients of the excitation mode. The modal-analysis representation is used to compute these coefficients for low- and high-loss samples with air gaps.**

**The "gap effect" is explained qualitatively by considering the influence of the dominant "slab mode," which focuses its energy into the dielectric slab, and the dominant "gap mode," which focuses its energy into the air gap.**

**An experimental approach, which consists of filling the air gap with conducting paste, is shown to essentially correct the problem altogether.**

### I. Introduction

The effect of the air gap in the characterization of high-dielectric materials, although not neglected (a number of perturbation techniques have been attempted [1]), has certainly been underestimated. Gaps on the order of a few percent, which are caused by imperfect sample fit in the waveguide, can produce errors on the order of 100 percent in the determination of the complex dielectric constant. The analysis reported here shows that, among many other effects, the inferred dielectric constant may even be larger than the true dielectric constant, a previously unsuspected result.

The experiment modeled in this work is performed using a rectangular waveguide excited by a $TE_{10}$ mode traveling in the $-z$ direction. A dielectric slab cut to the guide dimensions is placed in the guide and the reflected and transmitted powers are measured as a function of frequency. The geometry treated here, shown in Fig. 1, allows the sample to fit imperfectly into the guide by having a height smaller than that of the waveguide, while the sample width is equal to the guide width. Gaps at the end of the sample, which occur when the sample width is not equal to the guide width, are believed to have a minimal effect on such measurements since the exciting $TE_{10}$ mode has a zero electric field at these walls. Measurements conducted by Champlin and Glover confirm this belief [2].

The calculation proceeds by writing down the waveguide modes for the filled and unfilled portions of the guide. Overlap integrals of these modes are calculated in order to satisfy the electric and magnetic field boundary conditions at the air–slab interfaces, and the reflectance and transmittance coefficients of the $TE_{10}$ wave are determined. Since this is a complete description of the problem, the accuracy of the solution for all gap sizes is only affected by the number of modes which are included in the calculation.

Manuscript received January 26, 1987; revised July 25, 1987 This work was supported in part by Rockwell International Science Center IR&D

The author was with the Rockwell International Science Center, Thousand Oaks, CA. He is now with National Patent Analytical Systems, Shrewsbury, NJ 07701

IEEE Log Number 8719437.

### II. Modal Analysis

Wexler [3] introduces a general method for solving waveguide discontinuity problems. The problem at hand is a degenerate case of Wexler's boundary reduction in which discontinuities are produced by the slab rather than a change in guide dimensions. Filled and unfilled portions of the guide are described by different sets of orthogonal modes, and these modes are then used in order to satisfy the continuity of the transverse electric and magnetic fields across the slab faces at $z = 0$ and $z = -t$.

Let

$$\vec{E}_t = (1+\rho)\, u_0 \vec{e}_{u0} + \sum_{i=1}^{\infty} u_i \vec{e}_{ui} \tag{1}$$

and

$$\vec{H}_t = (1-\rho)\, u_0 \vec{h}_{u0} - \sum_{i=1}^{\infty} u_i \vec{h}_{ui} \tag{2}$$

describe the total transverse electric and magnetic fields expanded in terms of the transverse fields of the waveguide modes $\vec{e}_{ui}(x, y, z)$ and $\vec{h}_{ui}(x, y, z)$ for $z > 0$. Here $u_i$ is the coefficient of the "unfilled" mode $i$, and $\rho$ the reflection coefficient of mode 0, the $TE_{10}$ excitation mode.

In general, similar field descriptions must be written for the $z < -t$ portion of the guide; however, the symmetry about the transverse plane at $z = -t/2$ allows the problem to be solved by considering only the $z = 0$ discontinuity. The problem is treated as an equivalent transmission line T network with upper-arm impedances $Z_{11} - Z_{12}$ and common branch impedance $Z_{12}$. These impedances can be computed by considering symmetric and antisymmetric excitations, that is, by applying open- or short-circuit conditions at the central plane [3].

A second exploitation of this symmetry appears in the form of the transverse fields in the filled portion of the guide, $0 > z > -t$,

$$\vec{E}_t = \sum_{j=1}^{\infty} f_j (1 + s_{jj})\, \vec{e}_{fj} \tag{3}$$

and

$$\vec{H}_t = \sum_{j=1}^{\infty} f_j (1 - s_{jj})\, \vec{h}_{fj} \tag{4}$$

where the fact that $s_{jk} = 0$ for $j \neq k$ has been used [3]. The scattering coefficient $s_{jj}$ is given by

$$s_{jj}^s = -s_{jj}^a = e^{-\gamma_{fj} t} \tag{5}$$

for symmetric and antisymmetric excitations, where $t$ is the length of the sample, $\gamma_{fj}$ is the propagation constant of the "filled" mode $j$, and $f_j$ is its coefficient. Letting $\rho^s$ and $\rho^a$ be the reflectance coefficients with these excitations, the reflectance and

0018-9480/88/0400-0752$01.00 ©1988 IEEE

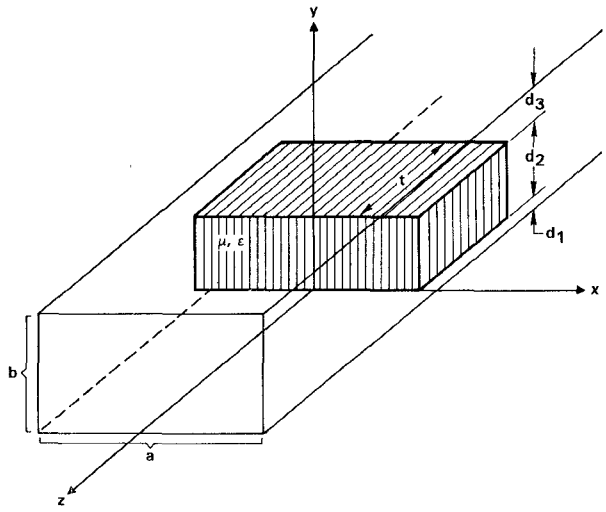


Fig. 1. Geometry of the dielectric slab in the waveguide.

transmittance of the $TE_{10}$ mode for the original problem are

$$\rho = \frac{\rho^s + \rho^a}{2} \quad \text{and} \quad \tau = \frac{\rho^s - \rho^a}{2}. \tag{6}$$

Given that the modes in the filled and unfilled sections satisfy the following orthogonality relations:

$$\int_A \vec{e}_{fj} \times \vec{h}_{fk} \cdot d\vec{A} = 0 \quad \text{and} \quad \int_A \vec{e}_{uj} \times \vec{h}_{uk} \cdot d\vec{A} = 0 \tag{7}$$

for $j \neq k$, then satisfying the continuity equations of the total transverse electric and magnetic fields of (1) to (4) across the discontinuity at $z = 0$ yields the equations

$$\left(1 + \rho^{s/a}\right) \int_A \vec{e}_{u0} \times \vec{h}_{u0} \cdot d\vec{A} = \sum_{j=0}^{\infty} \frac{f_j}{u_0} \left(1 + s_{jj}^{s/a}\right) \int_A \vec{e}_{fj} \times \vec{h}_{u0} \cdot d\vec{A} \tag{8}$$

and

$$\begin{aligned} &\left(1 + \rho^{s/a}\right) \int_A \vec{e}_{fn} \times \vec{h}_{u0} \cdot d\vec{A} \\ &\quad = \left(1 - s_{nn}^{s/a}\right) \frac{f_n}{u_0} \int_A \vec{e}_{fn} \times \vec{h}_{fn} \cdot d\vec{A} \\ &\qquad + \sum_{j=0}^{\infty} \frac{f_j}{u_0} \left(1 + s_{jj}^{s/a}\right) \sum_{i=1}^{\infty} \frac{\int_A \vec{e}_{fj} \times \vec{h}_{ui} \cdot d\vec{A} \int_A \vec{e}_{fn} \times \vec{h}_{ui} \cdot d\vec{A}}{\int_A \vec{e}_{ui} \times \vec{h}_{ui} \cdot d\vec{A}} \end{aligned} \tag{9}$$

where the integrals run across the waveguide cross section $A$, $-a/2 \leqslant x \leqslant a/2$ and $-b/2 \leqslant y \leqslant b/2$. The coefficients $u_i$ have been eliminated from these equations, which can now be used to solve for the unknown coefficients $f_j$ and $\rho$.

## III. Modes

The modes for the filled portion of the guide have been classified [4] as LSM (longitudinal-section magnetic) and LSE (longitudinal-section electric) waves. Although the usual set of TE and TM modes could be used to describe the unfilled portion of guide, the problem formulation is clearer if LSM and LSE modes are used in both sections. (If the guide width $a$ is allowed to tend toward infinity with this formulation, the geometry becomes that of parallel plates, and the complete problem can be described using only LSM modes in both sections of the plates.) The excitation mode is now the $LSM_{10}$ mode, which is equivalent to the $TE_{10}$ mode.

It should be noted that the well-known trick [5] of solving a waveguide problem by solving the corresponding parallel-plate problem with $\lambda \to \lambda_g$ cannot be applied here because of the dielectric nature of the obstacle.

The electric and magnetic fields for the filled guide modes are given as follows:

LSM modes ($E$ waves):

$$\bar{\epsilon} \cdot \vec{E} = \epsilon_\perp \vec{\nabla} \times \vec{\nabla} \times \vec{\Pi}_e \quad \text{and} \quad \vec{H} = -i\omega\epsilon_0 \epsilon_\perp \vec{\nabla} \times \vec{\Pi}_e \tag{10}$$

with

$$\vec{\Pi}_e = \psi_e(x, y) e^{-\gamma z} \hat{y}. \tag{11}$$

LSE modes ($H$ waves):

$$\vec{E} = i\omega\mu_0 \mu_\perp \vec{\nabla} \times \vec{\Pi}_h \quad \text{and} \quad \bar{\mu} \cdot \vec{H} = \mu_\perp \vec{\nabla} \times \vec{\nabla} \times \vec{\Pi}_h \tag{12}$$

with

$$\vec{\Pi}_h = \psi_h(x, y) e^{-\gamma z} \hat{y} \tag{13}$$

where

$$\bar{\epsilon} = \begin{pmatrix} \epsilon_\perp & 0 & 0 \\ 0 & \epsilon_\parallel & 0 \\ 0 & 0 & \epsilon_\perp \end{pmatrix} \qquad \bar{\mu} = \begin{pmatrix} \mu_\perp & 0 & 0 \\ 0 & \mu_\parallel & 0 \\ 0 & 0 & \mu_\perp \end{pmatrix} \tag{14}$$

and $\epsilon_\parallel = \epsilon_y$, $\epsilon_\perp = \epsilon_x = \epsilon_z$, $\mu_\parallel = \mu_y$, $\mu_\perp = \mu_x = \mu_z$.

This is a generalization of the field solutions given by Collin [6] and Gardiol [7] for anisotropic media. Modes for the cases when $\epsilon_x \neq \epsilon_z$ or $\mu_x \neq \mu_z$ cannot be derived from a single Hertzian potential.

The Hertzian potentials for these waves are defined as follows:

$$\vec{\Pi}_e = \psi_e(x, y, z) \hat{y} = -\left(\sqrt[4]{\frac{\mu_0}{\epsilon_0}} \Big/ \gamma_f^2\right) \cos\frac{\pi x}{a} f_e(y) e^{-\gamma_f z} \hat{y} \tag{15}$$

with

$$f_e(y) = \begin{cases} D_3 \cos p_a(b/2 - y) & b/2 - d_3 \leqslant y \leqslant b/2 \\ D_2 \cos(p_d y + \Delta) & -b/2 + d_1 \leqslant y \leqslant b/2 - d_3 \\ D_1 \cos p_a(b/2 + y) & -b/2 \leqslant y \leqslant -b/2 + d_1 \end{cases} \tag{16}$$

where the $y$ component of the wave vector in air ($a$) and dielectric ($d$) is

$$p_a^2 = \gamma_f^2 + k_0^2 - (\pi/a)^2 \tag{17a}$$

$$p_d^2 = \frac{\epsilon_\perp}{\epsilon_\parallel}\left[\gamma_f^2 + k_0^2 \mu_\parallel \epsilon_\parallel - (\pi/a)^2\right] \tag{17b}$$

and the continuity of the transverse fields at $y = -b/2 + d_1$ and $y = b/2 - d_3$ gives

$$\begin{aligned} 0 = \cos p_a d_3 &\left(\cos p_d d_2 \sin p_a d_1 + \frac{p_d}{\epsilon_\perp p_a} \sin p_d d_2 \cos p_a d_1\right) \\ - \sin p_a d_3 &\left(\frac{\epsilon_\perp p_a}{p_d} \sin p_d d_2 \sin p_a d_1 - \cos p_d d_2 \cos p_a d_1\right). \end{aligned} \tag{17c}$$

Similarly,

$$\vec{\Pi}_h = \psi_h(x,y,z)\,\hat{y} = -\left(\sqrt[4]{\frac{\epsilon_0}{\mu_0}}\Big/\gamma_f^2\right)\sin\frac{\pi x}{a} f_h(y)\,e^{-\gamma_f z}\hat{y} \quad (18)$$

with

$$f_h(y) = \begin{cases} D_3 \sin p_a(b/2-y) & b/2-d_3 \leqslant y \leqslant b/2 \\ D_2 \sin(p_d y + \Delta) & -b/2+d_1 \leqslant y \leqslant b/2-d_3 \\ D_3 \sin p_a(b/2+y) & -b/2 \leqslant y \leqslant -b/2+d_1 \end{cases} \quad (19)$$

where

$$p_a^2 = \gamma_f^2 + k_0^2 - (\pi/a)^2 \quad (20a)$$

$$p_d^2 = \frac{\mu_\perp}{\mu_\parallel}\left[\gamma_f^2 + k_0^2\mu_\parallel\epsilon_\parallel - (\pi/a)^2\right] \quad (20b)$$

and

$$0 = \cos p_a d_3\left(\cos p_d d_2 \sin p_a d_1 + \frac{\mu_\perp p_a}{p_d}\sin p_d d_2 \cos p_a d_1\right)$$

$$-\sin p_a d_3\left(\frac{p_d}{\mu_\perp p_a}\sin p_d d_2 \sin p_a d_1 - \cos p_d d_2 \cos p_a d_1\right). \quad (20c)$$

The complex transverse wavenumbers $p_a$ and $p_d$ are solutions to (17) and (20), the complex coefficients $D_3$, $D_2$, $D_1$, and $\Delta$ are found by satisfying the continuity of the $\vec{E}$ and $\vec{H}$ tangential field components at $y = b/2 - d_3$ and $y = -b/2 + d_1$, and $k_0 = 2\pi/\lambda$.

The following unitless parameters will be useful in describing the sample geometry:

$$\alpha = \frac{d_1 + d_3}{d_1 + d_2 + d_3} = \frac{d_1 + d_3}{b}$$

and

$$\Omega = \frac{d_1}{d_3} \qquad \text{with } d_1 \leqslant d_3.$$

$\alpha$ is the "gap size" and runs from zero, the case with no gap, to one, the case with no sample. $\Omega$ describes the "registration" of the sample within the guide and runs from zero, with the sample flush against the lower wall, to one, with the sample centered in the guide.

*Mode Types*

The LSM and LSE modes of this geometry were studied in detail by Pincherle [4] for lossless dielectric materials. He showed that as the dielectric constant is increased, the energy in these modes is focused into the high-dielectric material. However, when the sample is lossy, some of the modes focus their energy into the air gap instead of the dielectric material. (In the limiting case when the slab becomes an ideal conductor these modes become the modes of an unfilled waveguide of reduced height.) We shall refer to the modes that focus their energy into the dielectric material as slab modes and the modes that focus their energy into the air gap as gap modes. The distinction between these two types of modes is introduced only as a means for qualitatively describing the effect of the air gap. Both types of modes are solutions to the fundamental equations (16) and (19) and must be considered in the description of the total electric and magnetic fields.

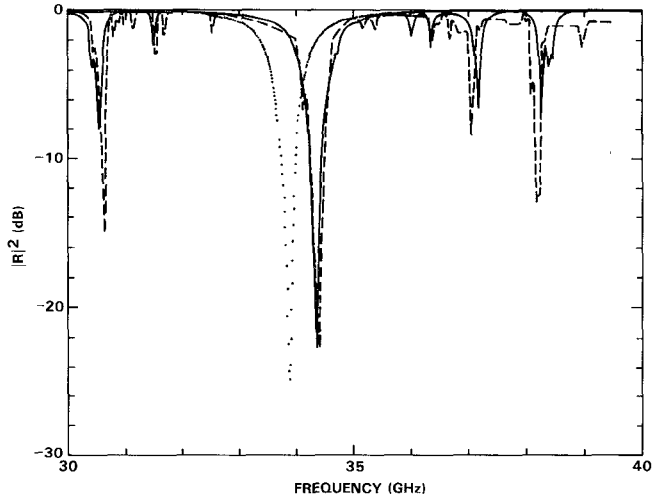


Fig. 2. Return loss spectrum for the $TiO_2$ sample: --- experiment; —— modal-analysis model; ····· model with no air gaps (calculated).

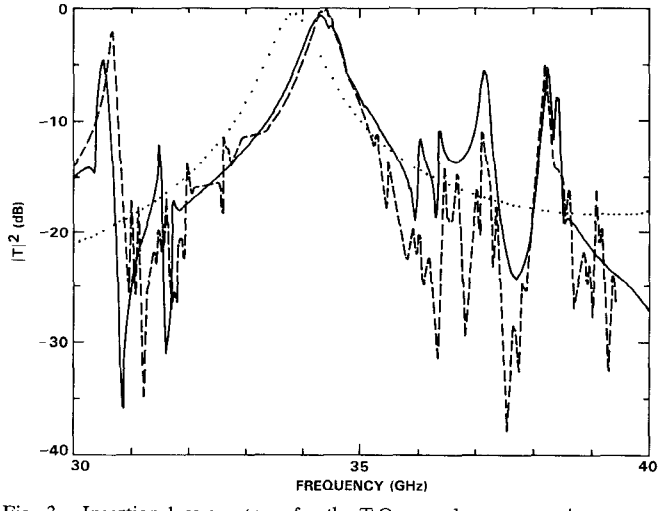


Fig. 3. Insertion loss spectrum for the $TiO_2$ sample: --- experiment; —— modal-analysis model; ····· model with no air gaps (calculated).

The lowest order slab mode has a propagation constant $\gamma \propto \sqrt{\epsilon\mu}$ like that of the $TE_{10}$ mode of a completely filled waveguide, and its attenuation is *increased* as the slab becomes more lossy. The lowest order gap mode, since it focuses its energy in the air gap, has a propagation constant like that of the $TE_{10}$ mode of an unfilled waveguide, and its attenuation is *decreased* as the slab becomes more lossy. The interplay of these two modes will help explain two sets of measurements on lossy dielectric samples in the next section.

The distinction between the two types of modes is lost for higher order modes; i.e., there is no dominant focus of the energy into either the air gap or the slab.

## IV. Comparison with Experiment

Two sets of waveguide measurements that illustrate the effect of the air gap on low-loss and high-loss dielectric samples are described below.

The first anomaly is illustrated in Figs. 2 and 3. These $|R|^2$ and $|T|^2$ measurements running from 30 to 40 GHz were on a $TiO_2$ single-crystal sample. A great deal of structure is present that cannot be attributed to the simple front and back face interference spectrum of the dominant mode. Also shown in Figs.

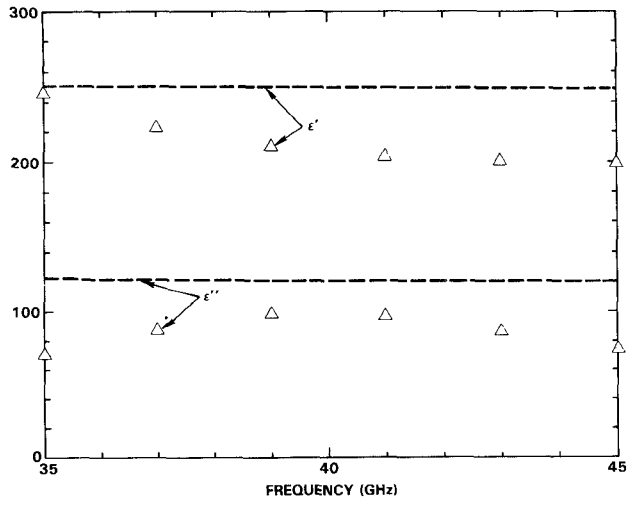


Fig. 4. Triangular points display the dispersion of the SBN complex dielectric constant. The dashed lines display the complex dielectric constant for a frequency-independent modal-analysis fit of the experimental data

2 and 3 are the $|R|^2$ and $|T|^2$ spectra produced by a best fit modal-analysis model as well as the theoretical spectra for the same slab with no gap.

$TiO_2$ is a very low loss, high dielectric material; consequently, there are many propagating modes within the slab. In the presence of the air gap these modes are strongly coupled to the excitation mode at particular frequencies, resulting in the exhibited resonance phenomenon. The frequency at which a particular resonance occurs is a function of $t$, $\alpha$, and $\Omega$ as well as both $\epsilon_{\|}$ and $\epsilon_{\perp}$, since $TiO_2$ is anisotropic.

Given that $t = 0.1073$ cm, the values $\epsilon_{\|} = 153.9 + 0.2i$, $\epsilon_{\perp} = 80.0 + 0.2i$, $\alpha = 2.48 \times 10^{-2}$, and $\Omega = 0.1$ were determined by matching the placement and magnitudes of the major resonance peaks of the experimental spectrum. If the real part of the dielectric constant had been calculated by noting the frequency at which $|R|^2$ is a minimum, then a value $\mathcal{R}(\epsilon_{\|}) = 152.7$, which is slightly lower than the true value $\mathcal{R}(\epsilon_{\|}) = 153.9$ calculated by the modal-analysis model, would have been obtained. However, if the sample had been situated nearly flush against the guide wall, $\Omega \approx 0$, the $|R|^2$ minimum would have shifted to a lower frequency than the no-gap case, thus predicting an erroneously high dielectric constant. The case in which the sample is completely flush against the guide wall is even more spectacular; the dominant peak ($|R|^2 \rightarrow 0$) is split into two equal peaks, one on each side of the no-gap dominant mode peak.

The differences between the model and experimental plots could be due to the nonrectangularity of the sample, gaps along the sides of the sample (which may account for some of the smaller resonances), and a nondiagonal $\bar{\epsilon}$ caused by a sample cut not exactly along the dominant axis.

It is readily noted that the presence of the air gap has not produced a drastic error in the determination of the dielectric constant. If, however, a spectrum had been taken that did not include the dominant mode peak, one of the other peaks could have been interpreted as such, and a very poor estimate for $\mathcal{R}(\epsilon_{\|})$ would have been obtained.

A second set of measurements, running from 35 to 45 GHz, on a high-loss strontium barium niobate (SBN) sample with $t = 0.0807$ cm is now considered. Interpretation of $|R|^2$ and $|T|^2$ data through consideration of the dominant mode only yields a dispersive dielectric constant, shown in Fig. 4, although it is believed that this material should have a relatively frequency independent dielectric constant over this band.

The modal-analysis fit with a frequency-independent dielectric constant yields $\epsilon_{\|} = 251 + 122i$, $\epsilon_{\perp} = 355 + 57i$, $\alpha = 1.48 \times 10^{-2}$, and $\Omega = 0.0$. Since the material is noticeably lossy, the previously described gap modes have begun to have an effect on the power distribution in reflection and transmission. A nonnegligible amount of energy, which normally would have been reflected by the dielectric in the no-gap case, is coupled into these modes, causing a reduction in the magnitude of $|R|^2$. The frequency dependence of $|T|^2$ is due to beating of the lowest order slab mode with the lowest order gap mode.

Although very little energy is initially coupled into the gap mode, it is only minimally attenuated during its propagation through the filled portion of the guide, while the slab mode, which initially carried most of the transmitted energy, is highly attenuated. Because of these offsetting effects, these two modes have coupled roughly the same amount of energy into the dominant mode transmitted wave of the unfilled region $z < t$. The difference in their propagation constants causes a rapidly varying phase difference as a function of frequency, which consequently causes the beating of the two waves.

## V. Corrections for the Air Gap

Simple perturbation formulas that attempt to correct for the effect of the air gap in waveguide dielectric measurements have been offered [1]. These expressions consider only the distorted $TE_{10}$ mode, and, consequently, are valid over a very small range of material parameters and gap sizes. The corrections offered by these formulas often produce errors larger than the uncorrected results.

An experimental approach, which consists of filling the air gap with a conducting paste, almost completely alleviates the effect of the air gap.

Measurements were taken on the $TiO_2$ and SBN samples with their air gaps filled with conducting paste. The resulting $TiO_2$ spectrum was almost identical to the no-air-gap spectra shown in Figs. 2 and 3. (Only three extraneous resonances were present and all had a magnitude less than 0.5 dB.) The resulting SBN spectrum, when interpreted with the dominant mode only, yielded a dielectric constant within 1 percent of its true value.

The filled-gap geometry was treated with the modal-analysis model and corroborated the findings of the experiments. The geometry for this model is that of a waveguide with a reduced cross section from $z = 0$ to $z = -t$. The offending gap modes have been removed, and the dominant mode is the $TE_{10}$ mode in a waveguide of reduced height, $b(1 - \alpha)$. Thus, when $\alpha \ll 1$, the effect of the filled gap is negligible.

## VI. Discussion

The determination of the dielectric constant for high-dielectric, lossless samples is not greatly affected by the presence of an air gap if enough of the frequency spectrum can be swept in order to ensure that the dominant mode interference spectrum can be identified. If one of the higher order mode resonances is incorrectly interpreted as the dominant mode resonance, then a very poor determination of the dielectric constant will be obtained. It should be noted that filling the air gap with an ideal conductor for such samples almost completely rids the spectra of the offending resonances.

The area in which air gaps are of the greatest concern seems to be in the measurement of lossy dielectric samples. It is in such samples that the gap modes drastically alter the power distribution of the reflection and transmission by allowing energy to seep around the sample. Simply taking more care in the sample

preparation does not seem to be an adequate solution, since gaps less than 1 percent cause significant errors in the determination of the dielectric constant.

The modal-analysis method presented here is very complicated, and it does not provide a reasonable method for analyzing waveguide dielectric measurements to determine sample permittivity. It is hoped, however, that this analysis has shown that even very small air gaps must be taken seriously in any experiment of the type presented here.

Simple perturbation formulas that relate the "measured" dielectric constant to the "actual" dielectric constant often produce worse results than just accepting the measured value as the true value. The best way of correcting for the air gap, it would seem, is to fill the gap with a conducting paste. The resulting measurements produce inferred dielectric constants that are very close to the true values so long as the gap is small.

## ACKNOWLEDGMENT

The author wishes to thank Dr. W. F. Hall, who originally pointed out the problem and who, through his subtle suggestions, ensured that this work became a thorough analysis. The author also wishes to thank Dr. W. Ho, who conducted the waveguide measurements on the SBN and $TiO_2$ samples and provided many insightful discussions. Dr. Ho suggested the experimental approach for the correction of the gap effect, which consists of filling the gaps with conducting paste.

## REFERENCES

[1] K. S Champlin and G. H Glover, "'Gap Effect' in measurements of large permittivities," *IEEE Trans Microwave Theory Tech.*, vol MTT-14, pp. 397–398, Aug. 1966.
[2] K S. Champlin and G. H. Glover, "Influence of waveguide contact on measured complex permittivity of semiconductors," *J. Appl Phys.*, vol 37, pp. 2355–2360, May 1966.
[3] A. Wexler, "Solution of waveguide discontinuities by modal analysis," *IEEE Trans. Microwave Theory Tech.*, vol MTT-15, pp 508–517, Sept. 1967.
[4] L Pincherle, "Electromagnetic waves in metal tubes filled with two dielectrics," *Phys. Rev.*, vol 66, pp. 118–130, Sept 1944
[5] L. Lewin, *Advanced Theory of Waveguides*. London: Iliffe & Sons, p 37.
[6] R. Collin, *Field Theory of Guided Waves*. New York: McGraw-Hill, 1960, ch. 6
[7] F. E. Gardiol, "Higher-order modes in dielectrically loaded waveguides," *IEEE Trans. Microwave Theory Tech.*, vol. MTT-16, pp. 919–924, Nov. 1968.

# Large-Signal Time-Domain Simulation of HEMT Mixers

GUAN-WU WANG, IKUROH ICHITSUBO, MEMBER, IEEE, WALTER H. KU, YOUNG-KAI CHEN, AND LESTER F. EASTMAN, FELLOW, IEEE

***Abstract*—A large-signal HEMT model and a time-domain nonlinear circuit analysis program have been developed. In this work a systematic method to simulate HEMT mixers and design them for maximum conversion gain is presented. The transconductance-compression effect reduces the mixer's conversion gain at high frequencies. Simulation results from mixers designed to operate at 10, 20, and 40 GHz show that a reduction in parasitic conduction in the AlGaAs layer significantly increases the conversion gain.**

Manuscript received July 10, 1987; revised December 3, 1987.

G.-W. Wang, Y.-K. Chen, and L. F. Eastman are with the School of Electrical Engineering, Cornell University, Ithaca, NY 14853.
I. Ichitsubo was with the School of Electrical Engineering, Cornell University, Ithaca, NY. He is now with Toshiba Corporation, Tokyo, Japan.
W. H. Ku was with the School of Electrical Engineering, Cornell University, Ithaca, NY. He is now with the Department of Electrical Engineering, University of California at San Diego, La Jolla, CA.

IEEE Log Number 8719438

## I. INTRODUCTION

The high electron mobility transistor (HEMT) is superior to the GaAs MESFET when used in low-noise microwave amplifiers. Recently the power performance of HEMT's with a single heterojunction [1] and double heterojunctions [2] have been investigated. Maas reported a HEMT mixer that operates at 45 GHz [3]. These promising results indicate that the HEMT will no longer be confined to small-signal applications.

For both the small-signal and the large-signal application of GaAs FET's, computer-aided design (CAD) is very valuable in the design process, especially in the design of monolithic integrated circuits, where tuning the circuits to optimize performance is impractical. The accuracy and efficiency of computer aided design and simulation rely on a well-developed device model. In this paper we present a large-signal HEMT model and a systematic CAD method in the time domain for the design and simulation of HEMT mixers. The effect on mixer performance by transconductance compression, which is a distinct feature of the HEMT [4], has also been studied.

## II. A LARGE-SIGNAL MODEL OF THE HEMT

Under large-signal operation, the element values of the HEMT equivalent circuit vary with time and become dependent on the terminal voltages. A large-signal model can be derived by considering the main nonlinear elements of the equivalent circuit. As shown in Fig. 1, the elements of the large-signal HEMT model assumed to be nonlinear in this work are the gate-to-source capacitance, $C_{gs}$, and the drain current source, $I_d$. Other circuit elements are assumed to be linear.

The drain current source is represented by the current–voltage equations derived in [5]. From the experimental results, $C_{gs}$ of a HEMT behaves quite similarly to that of a MESFET [6], [7], because considerable charges in addition to the two-dimensional electrons are modulated by the terminal voltages. Hence a valid approach is to use a Schottky diode equation and

$$C_{gs}(V_g) = \frac{C_{gs0}}{\left(1 - \frac{V_g}{V_{bi}}\right)^m} \tag{1}$$

where $C_{gs0}$ and $m$ are model parameters adjusted to fit the measured values. $V_{bi}$ is the built-in voltage for the Schottky gate and $V_g$ is the internal gate voltage.

Compared to the large-signal MESFET models given in [8] and [9], two diodes representing forward gate conductive current and gate–drain breakdown current are neglected in our HEMT model; hence this model is valid only when these two currents are absent in device operation, e.g., in a mixer. The nonlinearity of gate-to-drain capacitance, $C_{dg}$, is also neglected [7].

A GE HEMT with 0.25 $\mu$m gate length and 150 $\mu$m gate width was chosen [1]. Bias-dependent $S$ parameters and dc characteristics were used to construct the large-signal model. Small-signal equivalent circuits were extracted from the measured $S$ parameters at two bias points: $V_{GS} = -0.2$ V, $V_{DS} = 2.0$ V and $V_{GS} = -0.5$ V, $V_{DS} = 2.0$ V. $C_{gs0}$ and $m$ in (1) were determined by a